

An improved hyperelasticity relation in modeling viscoelasticity response of natural and high damping rubbers in compression: experiments, parameter identification and numerical verification

A.F.M.S. Amin¹, M.S. Alam, Y. Okui^{*}

Department of Civil and Environmental Engineering, 255 Shimo Okubo, Saitama University, Saitama 338-8570, Japan

Received 30 July 2001

Abstract

The rate-dependent behavior of natural and high damping rubbers is investigated in the compression regime. The experimental results demonstrate the prominence of the rate-dependent high initial stiffness feature in high damping rubber at low stretch level. A modified hyperelastic model is proposed to represent the rate-independent elastic responses including the high initial stiffness feature. A comparative evaluation is carried out to display the better performance of the proposed hyperelastic model than conventional ones over the strain range in representing the equilibrium and the instantaneous responses. The hyperelastic model is incorporated in a finite deformation rate-dependent model structure. A parameter identification scheme is proposed to identify the parameters for the equilibrium and instantaneous responses from the experimental data. The difficulties of direct application of infinitely fast or slow loading rate to such highly viscous materials to obtain these responses and thereby to identify the nonlinear elastic parameters are overcome. The proposed scheme is applied to three types of specimens including natural rubber and high damping rubber. Finally, numerical results obtained from the finite deformation rate-dependent model are compared with the test results to verify the adequacy and robustness of the proposed parameter identification scheme. © 2002 Elsevier Science Ltd. All rights reserved.

Keywords: Natural rubber; High damping rubber; High initial stiffness; Hyperelasticity; Equilibrium response; Instantaneous response; Viscoelasticity

1. Introduction

Vulcanized natural rubber (NR) has wide engineering applications such as shock absorbers, tunnel linings, bridge and building bearings, wind shoes, etc. (Ward, 1985; Roeder and Stanton, 1983). Furthermore, high damping rubber (HDR) has been developed for specific applications in base

^{*} Corresponding author. Tel.: +81-48-858-3558x4659; fax: +81-48-858-7374.

E-mail address: okui@koz.struct.civil.saitama-u.ac.jp (Y. Okui).

¹ Present address: Department of Civil Engineering, Bangladesh University of Engineering and Technology, Dhaka 1000, Bangladesh.

isolation bearings to protect structures from earthquakes (Kelly, 1997) and vibrations (Castellani et al., 1998). The mechanical behavior of these rubbers is dominated by nonlinear rate-dependent response (Aklonis et al., 1972) that includes other inelastic behavior such as Mullins' effect (Mullins, 1969) and hysteresis (Gent, 1962). These effects are said to be more evident in HDR. Hence, to reproduce the general mechanical behavior of NR and HDR under cyclic loading, there is necessity to develop a constitutive model that can simulate the rate-dependent nonlinear response including hysteresis. Although the final goal of this research is towards constructing a constitutive model representing all these aspects, as the first step, this paper focuses on modeling of the nonlinear viscoelastic behavior.

Fig. 1 presents a schematic representation of typical rate-dependent responses obtained from a viscoelastic solid. When the viscoelastic solid is loaded at an infinitely slow rate, the stress-strain curve follows the $E-E'$ path. This behavior is called the equilibrium response. On the other hand, in the case of infinitely fast loading, the response takes the $I-I'$ path. Such a response is known as the instantaneous response (Huber and Tsakmakis, 2000). Both equilibrium and instantaneous responses are elastic and they bind the viscosity domain. The area of viscous domain is directly related to the extent of material viscosity. Hence, one of the ways to develop a physically

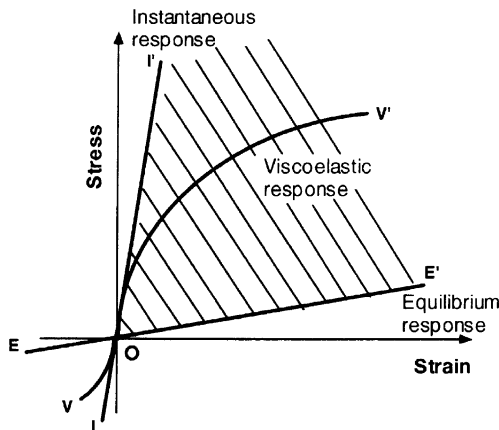


Fig. 1. Typical responses from a viscoelastic solid.

meaningful constitutive model is to include parameters that will directly express the instantaneous and equilibrium behaviors of the material. In this context, a standard three-parameter parallel model as illustrated in Fig. 2 can be considered. In such a physically motivated model, the first branch comprising of a spring (Element A) represents the equilibrium response, while the second branch comprising of a spring (Element B) and a dashpot (Element C) represents the 'overstress' feature resulting from the rate-dependent effect. In contrast to a constitutive model of linear viscoelasticity, however, nonlinear spring elements are required to represent the nonlinear equilibrium and instantaneous responses obtained from rubbers. In this context, an adequate hyperelastic model is vital to describe these two elastic boundary responses (Bonet and Wood, 1997).

Historically, the large extension feature of rubbery materials motivated researchers over decades to express the associated nonlinear elastic behavior through hyperelastic models (Charlton et al., 1993). Naturally, while formulating these relations, attention was paid mostly towards modeling of the response in the large strain tension regime. Among these conventional hyperelasticity models, strain-invariant based Mooney–Rivlin model (Mooney, 1940; Rivlin, 1948) is the oldest one. It performs only well up to moderate extension range, but cannot represent the strain-hardening feature typically exhibited by rubbers at a large strain level. Subsequently, Hart-Smith (1966), Alexander (1968), Yeoh (1990), Arruda

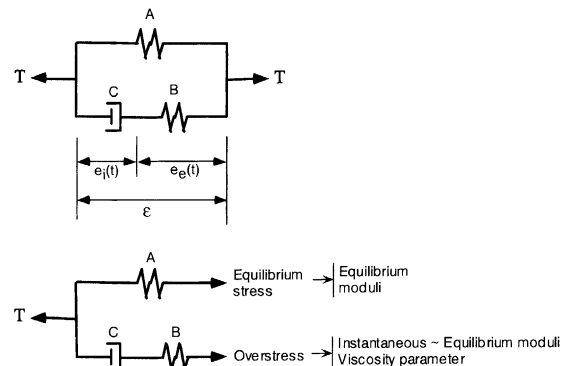


Fig. 2. Three-parameter parallel model.

and Boyce (1993), Yamashita and Kawabata (1992) proposed other improved models to include such a feature. Furthermore, stretch based models (Ogden, 1984; Peng and Landel, 1972) were also formulated. However, the performance of these models in representing compression response of NR is not yet investigated thoroughly. Besides this aspect, compared with NR, only limited experimental data on HDR have so far been reported (Dorfmann and Burtcher, 2000; Kelly, 1997; Hernandez, 1998). In general, HDR exhibits stronger nonlinearity at low strain levels. However, any study is yet to appear on the applicability of conventional hyperelastic relations to model HDR.

Moreover, in modeling viscoelastic response of rubbers, another obscurity exists in the parameter identification procedure. Figs. 1 and 2 have illustrated the definitions and roles of the equilibrium and instantaneous responses in a typical viscoelastic solid and material model. Yet, there are experimental limitations in applying infinitely slow or fast loading on a specimen to arrive at the equilibrium and instantaneous states, especially in case of highly viscous rubber-like materials. In this connection, the models of Lion (1996, 1997), Bergstrom and Boyce (1998), Miehe and Keck (2000) can be referred to where there exist direct references of the equilibrium and instantaneous states through the overstress concept. However, they had to depend on the numerical trials to identify the elasticity and viscosity parameters on the basis of the data of the experiments which were carried out at the middle of viscous domain. The parameters identified in this way, however, lose their physical meaning. On the other hand, Huber and Tsakmakis (2000) presented a formulation of finite deformation viscoelasticity laws that included direct expression of the equilibrium and instantaneous states. However, such theoretical work does not present any parameter identification procedure.

With this background, this paper presents an improved hyperelastic relation to represent nonlinear elastic response of NR and HDR in uniaxial compression. The relation is capable of including the initial stiffness feature present in the equilibrium and instantaneous states of the materials.

The new hyperelastic relation is incorporated in a finite deformation rate-dependent model structure, and a rate-dependent constitutive model is thereby derived. Furthermore, a parameter identification scheme is proposed to identify the parameters for the equilibrium and instantaneous responses from direct experimental observation. The scheme is applied on two different kinds of NRs and a HDR in order to observe the fundamental viscoelastic behavior of each material under compression and thereby to check the applicability of the proposed scheme under varied material types. In this course, the finite deformation viscoelasticity model is considered for determining the viscosity parameter from the experimental data. The performances of the conventional and the proposed hyperelastic models in representing equilibrium and instantaneous responses are compared. Finally, the adequacy of the proposed model and parameter identification scheme is verified by comparing experimental data with numerical results obtained from the finite deformation rate-dependent model using identified elasticity and viscosity parameters.

2. Experimental observation

In order to study the fundamental viscoelastic behavior of NR and HDR, an experimental scheme was applied on each of the three specimen types. The scheme comprises of a multi-step relaxation test, monotonic compression tests and simple relaxation tests. The tests were carried out in compression regime. To separate the Mullins' effect from the rate-dependent phenomena, preloading was applied on each specimen prior to the actual test. The following subsections present the details of the experiments.

2.1. Specimens

In the present study two different types of NR and a HDR were investigated. Table 1 presents the details of the specimens.

Apart from the difference in origin and end use, the microstructure of all these specimens also differs from each other. Fig. 3 shows the comparative microstructure of the specimens as visualized from

Table 1
Details of the specimens

	Specimen designation		
	NR-I	NR-II	HDR
Type	Natural rubber	Natural rubber	High damping rubber
Application	General purpose	Bridge bearing	Bridge bearing
Manufacturer	Shinoda Rubber Co.	Yokohama Rubber Co.	Yokohama Rubber Co.
Strength	4.0 MPa ^a	0.98 MPa ^b	0.78 MPa ^b
Shape	Cubic	Cylindrical	Cylindrical
Size	H : 50 mm, L : 50 mm, W : 50 mm	H : 41 mm, D : 49 mm	H : 41 mm, D : 49 mm

H : height, L : length, W : width, D : diameter.

^a Tensile strength.

^b Shear modulus tested according to JIS K 6301.

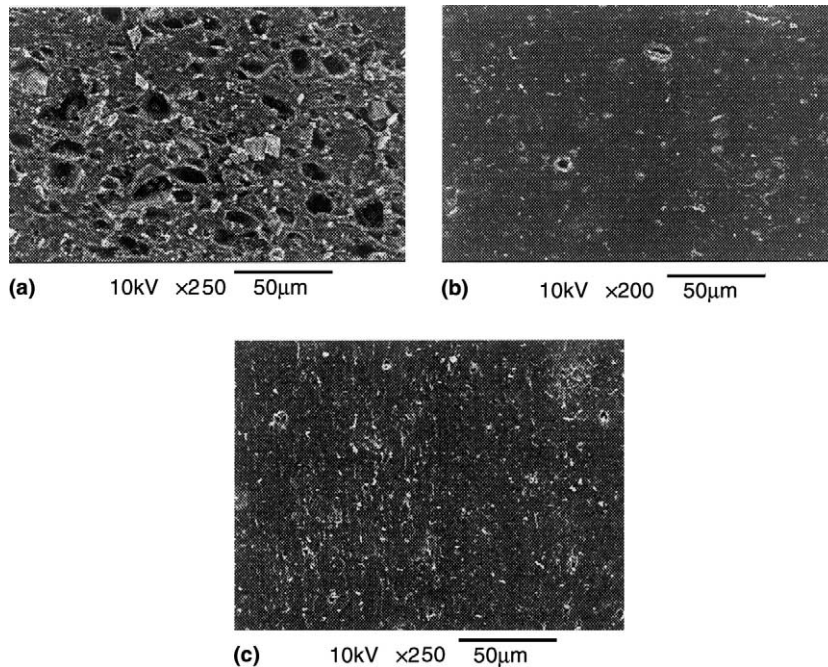


Fig. 3. Micro-graphs of: (a) NR-I; (b) NR-II; (c) HDR.

scanning electron microscope (SEM) observation. The observation was made in a Jeol JSM 5600LV machine. The SEM images illustrate a void dominated microstructure of NR-I in contrast to NR-II and HDR, where the occurrence of voids is rare.

2.2. Experimental set-up

A schematic detail of the experimental set-up is presented in Fig. 4. The specimens were tested in a

computer-controlled servo-hydraulic testing machine by using Shimadzu servo-pulser 4800 at room temperature. Displacement controlled tests in compression were carried out. The displacement was applied along the vertical axis of the specimen and a load cell measured the corresponding force. All data were recorded using a personal computer. In order to reduce the friction between sample and the plate and thereby to ensure a homogeneous deformation in the specimen, polypropylene films

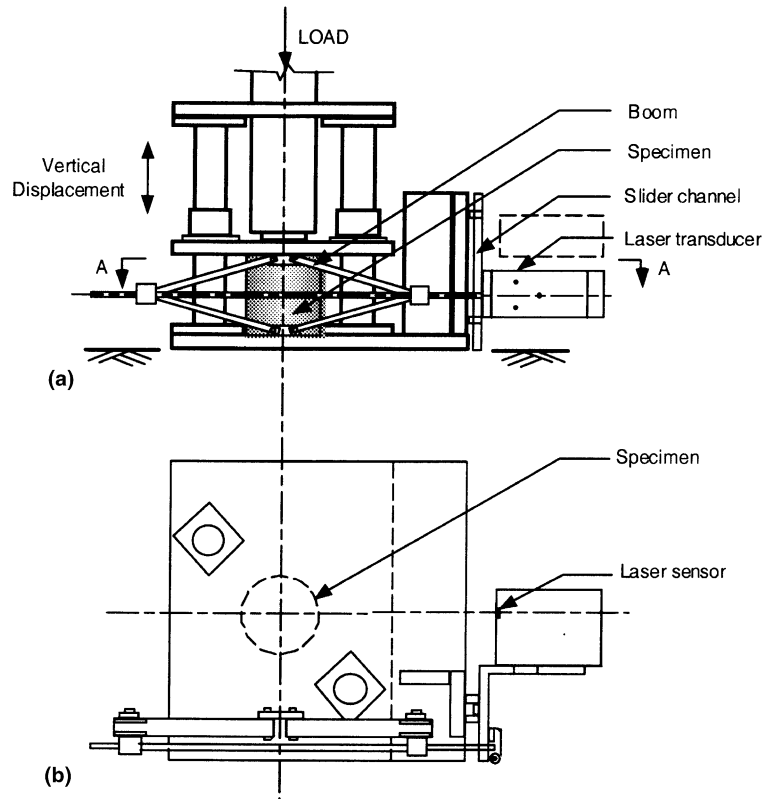


Fig. 4. Experimental set-up: (a) elevation; (b) section A–A.

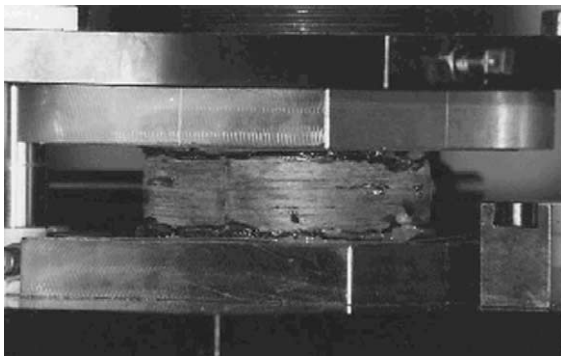


Fig. 5. Deformation homogeneity of HDR attained at 50% compressive strain.

with lubricant on the top and at the bottom of the sample were used. Fig. 5 illustrates the deformation homogeneity of a specimen that was ensured around 50% compressive strain level.

In general, rubbers are assumed to be incompressible materials. The Cauchy stress (true stress) can therefore be readily calculated from this assumption (Peeters and Kussner, 1999). However, SEM observations of the specimens of the present investigation have indicated the presence of microvoids. Hence to verify the assumption, the lateral displacement of the specimens was measured. A laser transducer (Ono Sokki LD-1110M-020) was used to measure the mid-height lateral displacement of the specimen surface. In fact, due to the very large applied vertical displacement (resulting up to 50% compressive strain), the midpoint of the specimen surface shifts significantly in the vertical direction from its initial position. To overcome this problem and to catch the midpoint of the deformed specimen, a special type of jig with a boom device was used to synchronize the position of the laser transducer with the applied displace-

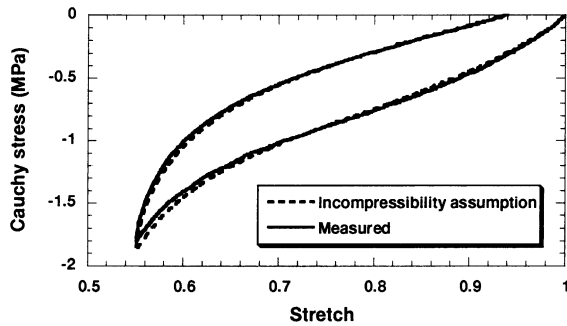


Fig. 6. Verification of incompressibility assumption through lateral displacement measurement in NR-I.

ment. Fig. 6 presents the measured Cauchy stress vs. applied stretch (i.e. $1 + dL/L$, where L is the undeformed length) response in comparison with that obtained by using the incompressibility assumption in NR-I. At a higher stretch level, there appears a little difference between the Cauchy stresses based on the measured lateral displacement and that obtained from the incompressibility assumption. However, the lateral displacement measurement indicates good reasoning for employing the incompressibility assumption. From now on in this paper, the applied stretch and the Cauchy stress of each test will be calculated under the assumptions of homogeneous deformation and incompressibility of the specimens.

2.3. Mullins' effect and preloading

Virgin rubber typically exhibits a softening phenomenon, known as Mullins' effect (Mullins, 1969) in the first loading cycle. The stress response depends on the past maximum strain. Mullins' effect was found to be present in all the specimens at the virgin state. Fig. 7 shows the relationship between the Cauchy stress and the stretch observed in the virgin NR-I. In order to remove Mullins' effect as well as obtain stable material behavior, all virgin specimens were subjected to a specified preloading sequence prior to actual tests. This approach of removing Mullins' effect from other phenomena is conceptually similar to that of Yeoh (1990), Yamashita and Kawabata (1992), Lion (1996, 1997), Bergstrom and Boyce (1998) and Miehe and Keck (2000). In the preloading,

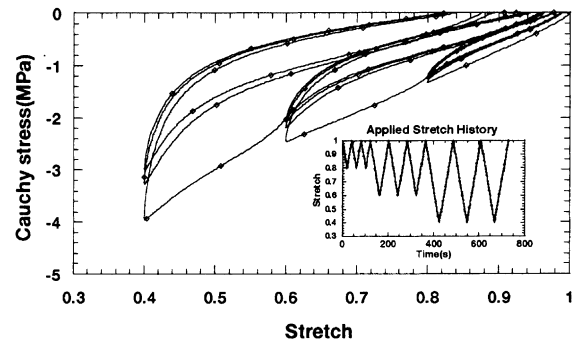


Fig. 7. Typical Mullins effect observed in NR-I.

each virgin specimen was subjected to cyclic uniaxial compressive loading for 5 cycles at 0.5 maximum stretch level with a stretch rate of 0.01/s.

Fig. 8 presents typical stress–stretch responses obtained from pre-loading tests for NR-I, NR-II and HDR. The softening behavior in the first loading cycle is evident from the figure. In NR-I and HDR, the softening behavior is more pronounced than that in the NR-II. All the specimens showed a repeatable stress–stretch response after passing through 2–3 loading cycles. However, Mullins' softening effect in a specimen recovers slowly with time. It is known as the 'healing effect' (Bueche, 1961). To keep this healing effect constant for each specimen, 20 min time interval was maintained between the pre-loading and the actual test for each specimen as described in the following sections. Apart from Mullins' effect, the typical strain-hardening feature of virgin rubbers at higher strain levels is more visible in NR-I and HDR than that in the NR-II.

2.4. Multi-step relaxation test

Fig. 1 presented the definition of the equilibrium response that can be obtained when the material is loaded at an infinitely slow rate. However, in rubbers, the presence of a significant, but unknown extent of material viscosity makes it difficult to specify a loading rate that is slow enough for obtaining the equilibrium response. To overcome this problem, a multi-step relaxation test was employed in this study to obtain the equilibrium response. This approach eliminates the

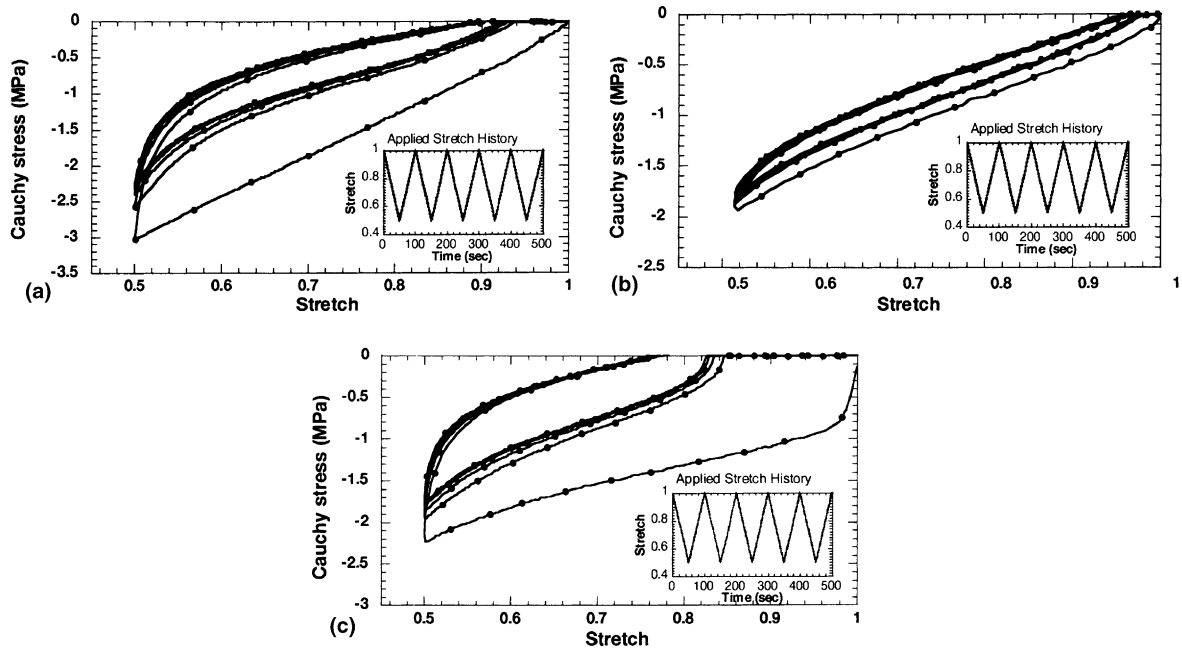


Fig. 8. Applied stretch history and stretch–stress response observed in pre-loading: (a) NR-I, (b) NR-II, (c) HDR.

necessity of performing uniaxial test trials in specifying a slow loading rate. In the present study, NR-I, NR-II, and HDR were tested up to 0.55, 0.50 and 0.50 stretch levels, respectively. Fig. 9 presents the applied stretch and the resultant stress histories of the tests. It is observed that at the end of each relaxation interval of 10 min duration, each stress history converges to an almost constant state in all specimens. Although the equilibrium state can be achieved only in an asymptotic sense, the stress states invariably indicate the neighborhood of the equilibrium states. In a consideration similar to Lion (1996, 1997), these stress states are regarded as the equilibrium states at respective stretch levels.

2.5. Monotonic compression test

The instantaneous elastic response of a solid is ideally obtained when the material is loaded at infinitely fast rate (Fig. 1). From an experimental point of view, however, there exists a finite maximum value of stroke rate for any displacement controlled loading device. Although, the use of a smaller specimen dimension in the loading direc-

tion can increase the loading rate on a specimen, the reduced aspect ratio of the specimen increases the boundary effects on the other turn. Hence, to find out a method for estimating the instantaneous response, a series of monotonic compression tests were conducted. The tests were carried out at different constant strain rates up to 0.5 stretch level. In the test series, a number of constant stretch-rate cases within the range $0.001\text{--}0.96\text{ s}^{-1}$ were considered.

Fig. 10 shows the rate-dependent Cauchy stress–stretch responses that were observed in six stretch rate cases for NR-I and four stretch rate cases for each of the other two specimens. In general, the stress responses contain a threefold feature, which is high initial stiffness at a low strain level followed by noticeable large compressibility at moderate strain and large-strain hardening at the end part. These observations will be discussed once again in Section 3.1 to derive an adequate hyperelastic relation to represent all these aspects. When compared among the three specimens, the high initial stiffness at the low stretch level is the most prominent in HDR at higher stretch rate. The cause of such characteristic nonlinearity is

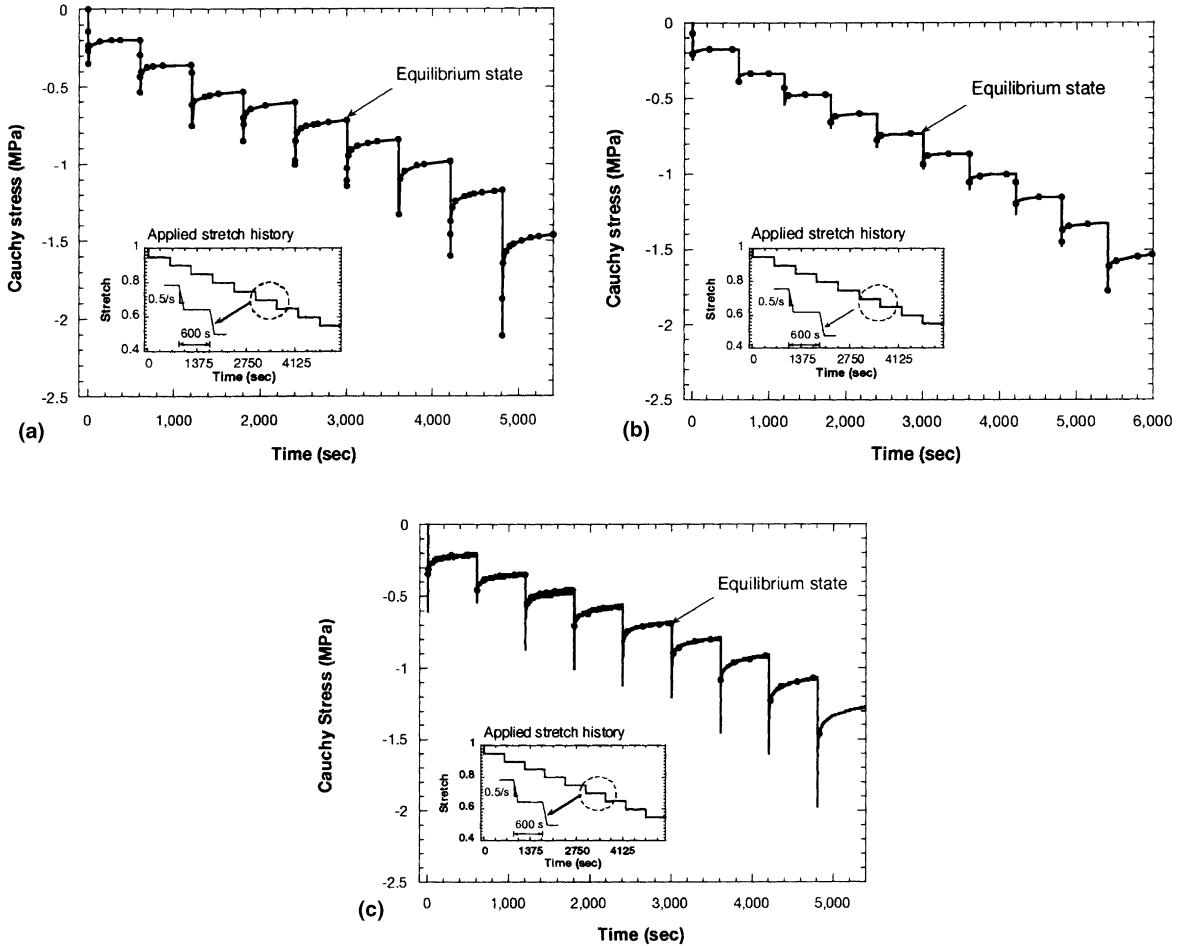


Fig. 9. Applied stretch history and stretch–stress response observed in multi-step relaxation test: (a) NR-I, (b) NR-II, (c) HDR.

attributed to the presence of very high amount of fillers added to produce HDR (Kelly, 1997; Dorfmann and Burtcher, 2000). However, a weaker strain hardening feature in NR-II than that of the other two specimens at higher stretch levels is also noticeable.

A further comparison of the responses at different stretch rates for each specimen shows that, with increasing stretch rate, the stresses increase due to viscosity effect. At higher stretch rates, however, a diminishing trend in the increase of stress response was observed indicating the approach of an instantaneous state in all specimens. Hence, for NR-I and HDR, the stress responses obtained at more than 0.47/s stretch rate can be

considered as the neighborhood of the instantaneous state. For NR-II, the corresponding stretch rate is 0.075/s. The observation of viscosity induced rate-dependent phenomenon in rubbers under monotonic loading was also reported in the works of Lion (1996, 1997); Bergstrom and Boyce (1998); Miehe and Keck (2000). However, these observations could not identify the existence of instantaneous state. In contrast, the present experimental work reports the observation of such fundamental viscoelastic phenomenon in NR and HDR.

To illustrate the existence and extent of viscous domain in each material, the equilibrium loci obtained from Section 2.4 were compared here with the experimental results of monotonic compres-

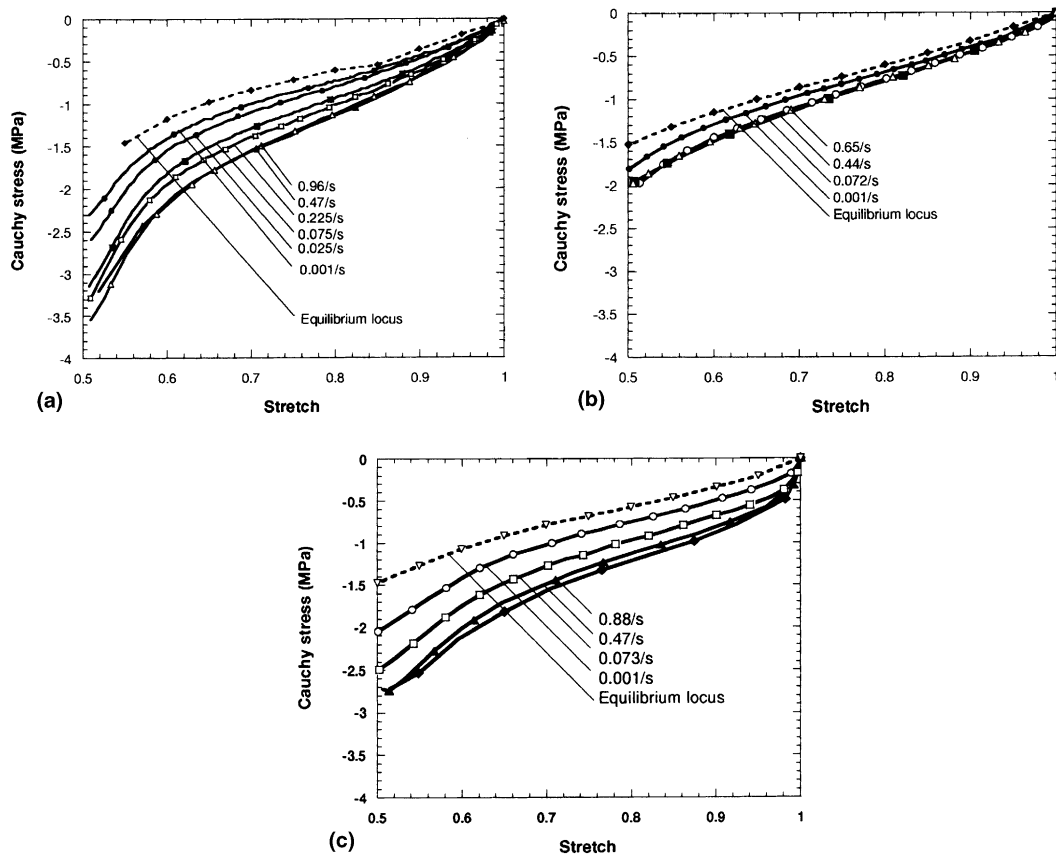


Fig. 10. Comparison of monotonic compression test stretch–stress responses at different stretch rates along with the equilibrium locus: (a) NR-I, (b) NR-II, (c) HDR.

sion tests. The locus plotted in Fig. 10 represents the equilibrium state boundary of the viscous domain for each material. Comparisons of the Fig. 10(a)–(c) show that the equilibrium loci estimated for all the specimens are comparable. However, the stress response of NR-II at faster stretch rates is much lower than those of NR-I and HDR. This results in a much smaller viscous domain for NR-II characterizing low material viscosity. The striking difference in viscoelasticity property in NR-I and NR-II can be related to the presence of voids in the microstructure of NR-I.

2.6. Simple relaxation test

The multi-step relaxation test and the monotonic compression tests described in Sections 2.4

and 2.5 enabled to estimate the instantaneous and the equilibrium responses. The remaining problem is to characterize the viscosity property. To this end, a series of simple relaxation tests at different stretch levels were carried out. In this course, a stretch rate of 0.5/s followed by a hold time of 10 min was used in all the tests described in this section.

Fig. 11 shows the stress histories obtained from the tests on NR-I at 0.7 stretch, and on NR-II and HDR at 0.5 stretch level. For NR-I and HDR, rapid stress relaxation was displayed in the first 2 min of hold time after which it approached asymptotically towards an equilibrium state within next 2 min. The amount of stress relaxation of NR-II was found much lower than that of the other specimens. The smaller area of viscous do-

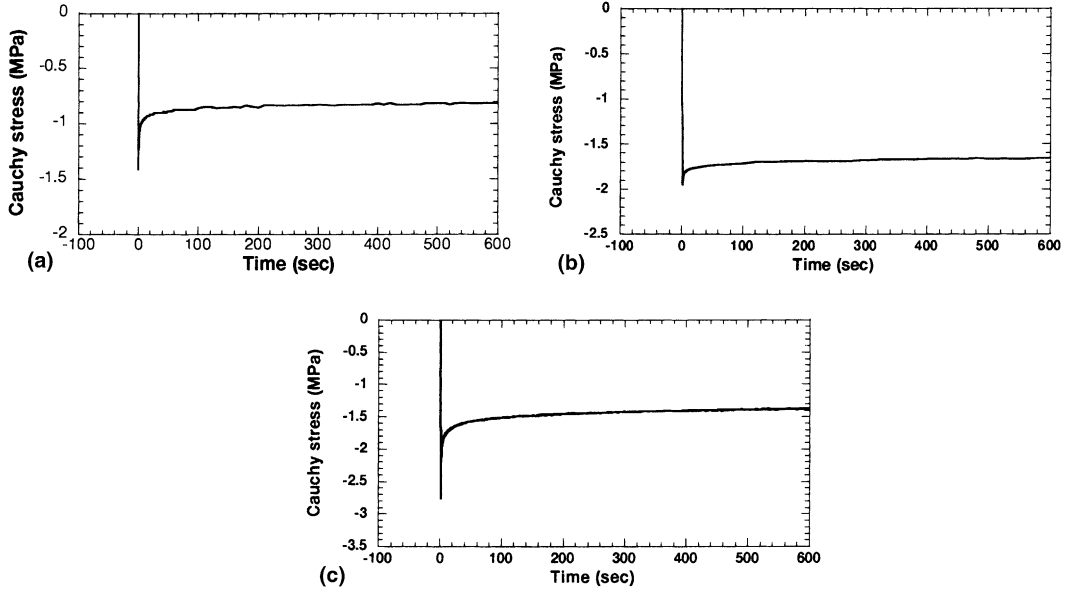


Fig. 11. Stress history obtained from simple relaxation test: (a) NR-I, (b) NR-II, (c) HDR.

main as observed in NR-II (Fig. 10(b)) has a direct conformity with this stress relaxation test result. This observation conforms to the viscous domain characteristics of the material as mentioned in Section 2.5. However, the amount of stress relaxation in each specimen was found not to vary with the change of stretch levels. The simple relaxation tests at other but different stretch levels have confirmed this fact. For space limitation of this paper, presentation of those data is being skipped.

3. Constitutive modeling

The experimental observation (summarized in Section 2) revealed a strong nonlinearity in monotonic response along with significant strain-rate dependency feature. Typically, hyperelastic model are used to represent the response of rubbers at a particular strain rate assuming complete elastic recovery of the material (Bonet and Wood, 1997). However, in order to model the rate dependency, the hyperelastic models are required to be combined with a rate-dependent model (Fig. 2) to represent the equilibrium and instantaneous responses. To this end, this section proposes a hyperelastic

model and its incorporation into a rate-dependent model structure to derive the final model.

3.1. Hyperelasticity for equilibrium and instantaneous responses

For isotropic elastic materials, the strain energy function W can be expressed as a function of invariants of a deformation tensor I_i ($i = 1, 2, 3$),

$$W = W(I_1, I_2, I_3). \quad (1)$$

If the left Cauchy–Green deformation tensor \mathbf{B} is employed as the deformation tensor, the deformation invariants can be rewritten in terms of the principal stretches λ_i ($i = 1, 2, 3$),

$$\begin{aligned} I_1 &= \text{tr}\mathbf{B} = \lambda_1^2 + \lambda_2^2 + \lambda_3^2, \\ I_2 &= \frac{1}{2} \left\{ (\text{tr}\mathbf{B})^2 - \text{tr}(\mathbf{B}\mathbf{B}) \right\} \\ &= (\lambda_1\lambda_2)^2 + (\lambda_2\lambda_3)^2 + (\lambda_3\lambda_1)^2, \\ I_3 &= \det\mathbf{B} = (\lambda_1\lambda_2\lambda_3)^2. \end{aligned} \quad (2)$$

When the material is incompressible, the third invariant $I_3 = 1$, and W is represented as a function of I_1 and I_2 only,

$$W = W(I_1, I_2). \quad (3)$$

From Truesdell and Noll (1992), it follows that the Cauchy stress \mathbf{T} is expressed as

$$\mathbf{T} = -p\mathbf{1} + \mathbf{T}_E, \quad (4)$$

$$\mathbf{T}_E = 2\frac{\partial W}{\partial I_1}\mathbf{B} - 2\frac{\partial W}{\partial I_2}\mathbf{B}^{-1}, \quad (5)$$

where $\mathbf{1}$ is the identity tensor, p is the hydrostatic pressure, and the subscript ‘E’ denotes the deviatoric part.

From Eqs. (1)–(5) it becomes clear that the representation of incompressible hyperelastic material behavior is solely dependent on the definition of $W(I_1, I_2)$.

However, due to the strong dependence of the stress response on the state of strain, experiments are required to identify an adequate form of W . In this context, tests in uniaxial tension/compression, bi-axial tension and pure shear deformation modes were proposed in the early works of Rivlin and Saunders (1951). The main motivation of conducting tests at different deformation modes was to come up with a W function that is adequate enough in predicting material behavior in different deformation modes. Kawabata and Kawai (1977) and Kawabata et al. (1981) investigated the dependence of $\partial W/\partial I_1$ and $\partial W/\partial I_2$ on I_1 and I_2 using uniaxial and biaxial test data. They showed that $\partial W/\partial I_1$ and $\partial W/\partial I_2$ depend only on I_1 and I_2 , respectively. This led to the separation of W into two individual functions namely $f(I_1)$ and $g(I_2)$

$$W(I_1, I_2) = \int f(I_1) dI_1 + \int g(I_2) dI_2, \quad (6)$$

where

$$f(I_1) = \frac{\partial W}{\partial I_1}, \quad g(I_2) = \frac{\partial W}{\partial I_2}.$$

Lambert-Diani and Rey (1999) further considered this notion to propose a general procedure for identifying the strain energy density function. In their work, the effect of the maximum principal stretch, λ_1 on the values of I_1 and I_2 in uniaxial tension, pure shear and equi-biaxial tension modes were considered. It was concluded there that an experiment with either $\lambda_1 > 1$ or $\lambda_2 > 1$ is sufficient to determine $f(I_1)$. However, they clarified the necessity of an biaxial experiment with $\lambda_1 > 1$ and $\lambda_2 > 1$ for obtaining $g(I_2)$. As far as the prediction

of incompressible uniaxial deformation is concerned, it can be seen that from the condition of incompressibility, $I_3 = 1$ gives $\lambda_2 = \lambda_3 = \lambda_1^{-1/2}$. Therefore, for uniaxial compression, $\lambda_1 < 1.0$ gives $\lambda_2 > 1.0$ which is the sufficient condition to determine $f(I_1)$ as proposed by Lambert-Diani and Rey. In this paper, this condition has been utilized to modify the Yamashita and Kawabata (1992) model and thereby to propose the strain energy function in terms of I_1 for NR and HDR in uniaxial compression. Eq. (7) presents the proposed strain energy density relation as a function of I_1

$$W(I_1) = C_5(I_1 - 3) + \frac{C_3}{N+1}(I_1 - 3)^{N+1} + \frac{C_4}{M+1}(I_1 - 3)^{M+1}, \quad (7)$$

where C_5 , C_3 , C_4 , M , and N are material parameters with $N \geq 1.0$ and $0.0 \leq M \leq 1.0$. For uniaxial incompressible deformation, the expression of T_{11E} for the proposed function can be derived from Eq. (5) as

$$T_{11E} = 2\left(\lambda_1^2 - \frac{1}{\lambda_1}\right) [C_5 + C_3(I_1 - 3)^N + C_4(I_1 - 3)^M]. \quad (8)$$

It should be noted that the first term with coefficient C_5 is a component of original Mooney–Rivlin model (Mooney, 1940; Rivlin, 1948), while the term with C_3 and N coefficients was proposed by Yamashita and Kawabata to include the hardening feature observed at higher strain levels. In order to incorporate the initial stiffness part, we propose the incorporation of the third term associated with coefficient C_4 and M .

The hyperelasticity model proposed in this section will be used in the following section to describe the equilibrium and instantaneous responses in a viscoelasticity model. The identification of equilibrium and instantaneous responses from experimental data will be discussed in Section 4 together with their representation through the proposed hyperelasticity model.

3.2. Viscoelasticity modeling

Section 3.1 has introduced a hyperelasticity model to represent the elastic response obtained

from rubbers in uniaxial compression. In order to model the strain-rate dependency of NR and HDR, the proposed hyperelasticity relation will be employed to describe the equilibrium and instantaneous state boundaries that exist in the responses of any typical viscoelastic solid illustrated in Fig. 1. The total stress is decomposed into the equilibrium and viscosity induced overstress parts following the concept of the three parameter parallel model as shown in Fig. 2. The deformation gradient tensor \mathbf{F} is decomposed into $\mathbf{F} = \mathbf{F}_e \mathbf{F}_i$, where \mathbf{F}_e and \mathbf{F}_i are the deformation gradients associated with e_e and e_i , respectively. Similar approaches in the decomposition of deformation were also employed by Lubliner (1985), Le Tallac et al. (1993), Reese and Govindjee (1998), Huber and Tsakmakis (2000). In this decomposition \mathbf{F}_i component introduces an intermediate equilibrium configuration. The intermediate configuration is resulted, when the stress is unloaded at an infinitely fast rate to an equilibrium state keeping the value of \mathbf{F}_i at constant during the unloading process.

From the model structure shown in Fig. 2, the deviatoric part of the Cauchy stress tensor, \mathbf{T}_E can be decomposed into equilibrium part $\mathbf{T}_E^{(E)}$ and the overstress part $\mathbf{T}_E^{(OE)}$

$$\mathbf{T}_E = \mathbf{T}_E^{(E)} + \mathbf{T}_E^{(OE)}, \quad (9)$$

with

$$\mathbf{T}_E^{(E)} = 2 \frac{\partial W^{(E)}}{\partial I_{1B}} \mathbf{B} - 2 \frac{\partial W^{(E)}}{\partial I_{2B}} \mathbf{B}^{-1}, \quad (10)$$

$$\mathbf{T}_E^{(OE)} = 2 \frac{\partial W^{(OE)}}{\partial I_{1B_e}} \mathbf{B}_e - 2 \frac{\partial W^{(OE)}}{\partial I_{2B_e}} \mathbf{B}_e^{-1}, \quad (11)$$

where $\mathbf{B}_e = \mathbf{F}_e \mathbf{F}_e^T$, and I_{1B} and I_{2B} are the first and second invariant of \mathbf{B} . The subscript 'e' denotes the quantities related to \mathbf{F}_e .

From Huber and Tsakmakis (2000), the rate of left Cauchy–Green deformation tensor for the considered model is given by

$$\dot{\mathbf{B}}_e = \mathbf{B}_e \mathbf{L}^T + \mathbf{L} \mathbf{B}_e - \frac{2}{\eta} \mathbf{B}_e \left(\mathbf{T}_E - \mathbf{T}_E^{(E)} \right), \quad (12)$$

$$\mathbf{L} = \dot{\mathbf{F}} \mathbf{F}^{-1}, \quad (13)$$

where \mathbf{L} is the velocity gradient tensor. The (\cdot) indicates the material time derivative. η is the material viscosity represented by the dash-pot.

Substituting the proposed strain energy density function, Eq. (7) into Eqs. (9)–(12), we have the explicit expressions for \mathbf{T} and the rate of \mathbf{B}_e ,

$$\begin{aligned} \mathbf{T} = & -p \mathbf{1} + 2C_5^{(E)} \mathbf{B} + 2C_3^{(E)} (I_{1B} - 3)^{N^{(E)}} \mathbf{B} \\ & + 2C_4^{(E)} (I_{1B} - 3)^{M^{(E)}} \mathbf{B} + 2C_5^{(OE)} \mathbf{B}_e \\ & + 2C_3^{(OE)} (I_{1B} - 3)^{N^{(OE)}} \mathbf{B}_e \\ & + 2C_4^{(OE)} (I_{1B} - 3)^{M^{(OE)}} \mathbf{B}_e, \end{aligned} \quad (14)$$

$$\begin{aligned} \dot{\mathbf{B}}_e = & \mathbf{B}_e \mathbf{L}^T + \mathbf{L} \mathbf{B}_e \\ & - \frac{4}{\eta} \mathbf{B}_e \left(C_5^{(OE)} \mathbf{B}_e + C_3^{(OE)} (I_{1B} - 3)^{N^{(OE)}} \mathbf{B}_e \right. \\ & \left. - C_4^{(OE)} (I_{1B} - 3)^{M^{(OE)}} \mathbf{B}_e \right). \end{aligned} \quad (15)$$

The material parameters of the proposed model expressed in Eqs. (14) and (15) are summarized in Table 2.

4. Parameter identification

The experimental observations of Section 2 have revealed the viscoelastic property of NR and HDR, while Section 3 has presented a constitutive model derived from physical viewpoint of material behavior. At this stage, the interest of the work focuses on identifying the model parameters in an explicit way based on the experimental data. The following sections present the details of the proposed parameter identification scheme.

Table 2
Material parameters

Response components	Material parameters				
Equilibrium stress	$C_5^{(E)}$	$C_3^{(E)}$	$C_4^{(E)}$	$M^{(E)}$	$N^{(E)}$
Overstress	$C_5^{(OE)}$	$C_3^{(OE)}$	$C_4^{(OE)}$	$M^{(OE)}$	$N^{(OE)}$
Viscosity	η				

4.1. Elasticity parameters

4.1.1. Equilibrium response

The introduction of multi-step relaxation tests in Section 2.4 has eliminated the problems and subsequent uncertainties associated with specifying a slow loading rate on a rubbery material with unknown viscosity, and thereby to approximate the equilibrium locus (Fig. 10). At this point, the coefficients of the hyperelasticity relation (Eqs. (13) and (14) and Table 2) for the locus can be readily determined by a least-squares method. The values of the parameters are listed in Tables 3–5 for NR-I, NR-II, and HDR, respectively. Fig. 12 illustrates the representation of equilibrium locus by the hyperelasticity model. The adequate representation of the response at all stretch levels is evident.

4.1.2. Instantaneous response

The monotonic compression tests presented in Section 2.5 displayed a diminishing trend in the increase of the stress response at higher stretch rates indicating the approach of the instantaneous state. Interestingly, the overall stress-stretch response at each stretch rate has a characteristic curve, which can be described by the hyperelas-

ticity model. On the basis of this feature, the constants, i.e. C_5 , C_4 , and C_3 were determined for each monotonic compression test with different stretch rates ranging from 0.001/s to 0.96/s. In the Cauchy stress-stretch relation of the hyperelasticity model (Eq. (8)), each contribution from the second and third terms is related to two parameters, i.e. C_3 , N and C_4 , M , respectively. However, the values of M and N have a weaker sensitivity on the whole relation. Hence, constant values of M and N as determined from the equilibrium locus of each material were used for determining C_3 and C_4 parameters. The C_5 , C_3 , and C_4 parameters determined by this procedure are plotted in Fig. 13 against the corresponding stretch rate values.

It is interesting to note that the values of C_5 , C_3 and C_4 parameters (Fig. 13) follow an asymptotic trend with the increase of applied stretch rate. This must be due to the approach of the instantaneous state. For NR-I, such a feature is noticed over a stretch rate of 0.25/s, while for NR-II the corresponding stretch rate is 0.1/s. For HDR it is around 0.7/s. The parameters for the instantaneous response are estimated from this asymptotic trend within finite stretch rate region. The values obtained from the highest stretch rate case in each specimen and denoted by X_1 , X_2 and X_3 (Fig. 13)

Table 3
Elastic material parameters (NR-I)

Responses	C_5 (MPa)	C_3 (MPa)	C_4 (MPa)	M	N
Equilibrium	0.99	0.40	-0.89	0.25	1.00
Instantaneous	1.89	0.86	-1.80	0.25	1.00

Table 4
Elastic material parameters (NR-II)

Responses	C_5 (MPa)	C_3 (MPa)	C_4 (MPa)	M	N
Equilibrium	0.67	0.07	-0.31	0.25	1.00
Instantaneous	1.04	0.22	-0.68	0.25	1.00

Table 5
Elastic material parameters (HDR)

Responses	C_5 (MPa)	C_3 (MPa)	C_4 (MPa)	M	N
Equilibrium	0.79	0.18	-0.55	0.25	1.00
Instantaneous	2.35	0.74	-2.28	0.25	1.00

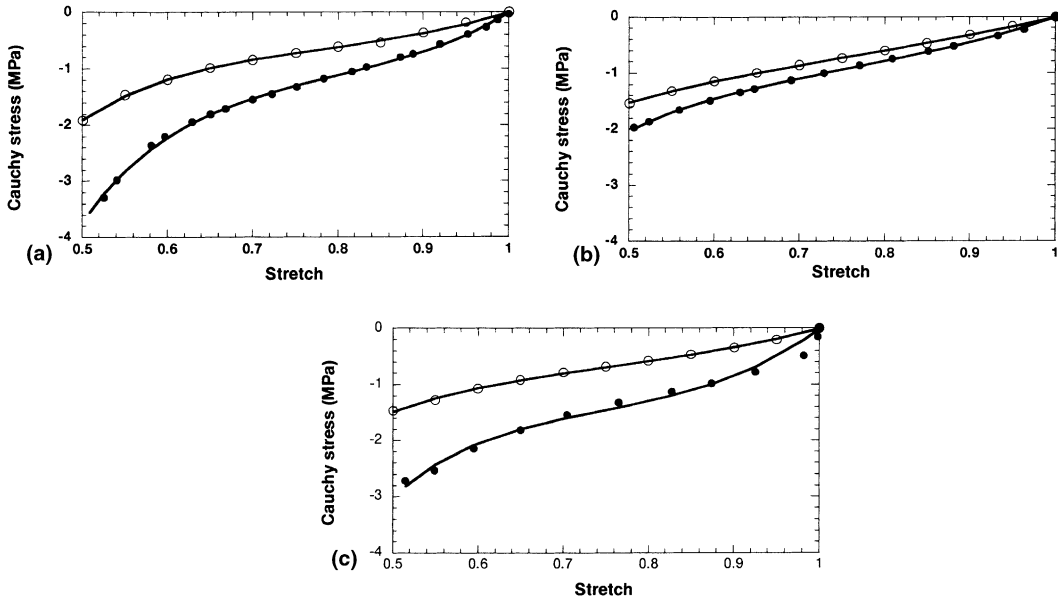


Fig. 12. Comparative representation of equilibrium and instantaneous response by the proposed hyperelastic model. (○) Equilibrium response obtained from experiment, (●) instantaneous response obtained from experiment, (–) proposed hyperelastic model representation: (a) NR-I, (b) NR-II, (c) HDR.

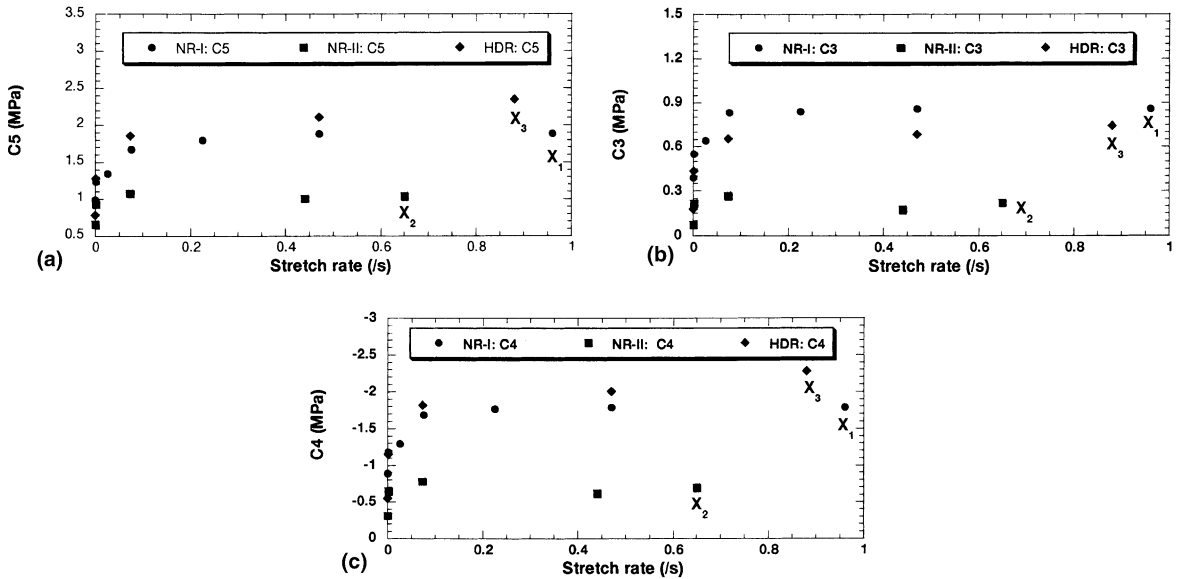


Fig. 13. Best-fit hyperelasticity coefficients for monotonic compression tests with different stretch rates: (a) C_5 , (b) C_3 , (c) C_4 values.

were taken for representing the instantaneous response. The values are presented in Tables 3–5. The subtraction of the values of C_5 , C_3 and C_4 from the instantaneous to the equilibrium state

gives the parameter values for the overstress response as mentioned in Table 2. Fig. 12 illustrates the representation of instantaneous response by the proposed hyperelasticity model where a good

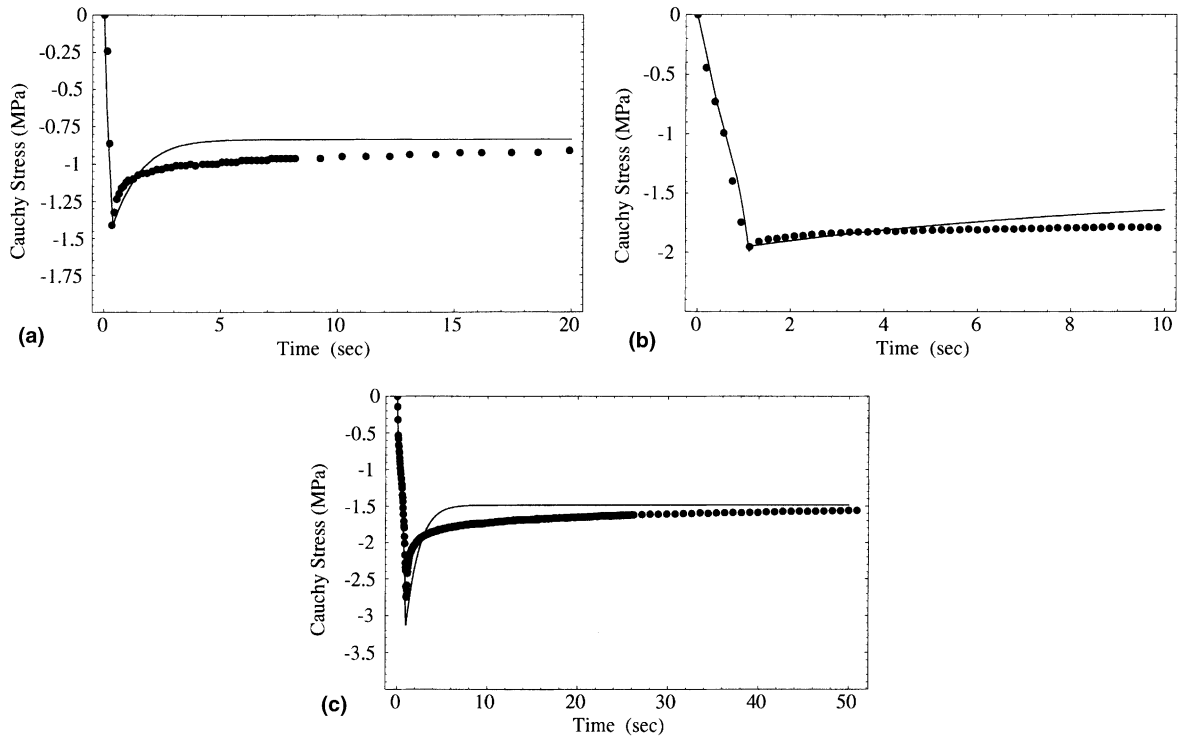


Fig. 14. Estimation of viscosity parameter by simulating the simple relaxation test result: (—) numerical simulation, (●) experiment. (a) NR-I, (b) NR-II, (c) HDR.

representation over the stretch range can be observed. The good performance of the model in capturing the high initial stiffness feature can be well noted.

4.2. Viscosity

The determination of elastic parameters completes the representation of the boundary of viscous domain and leaves the material viscosity η (Fig. 2) as the only unknown. In this situation, the results of simple relaxation tests were utilized (Section 2.6) to evaluate the viscosity parameter. In these tests, the loading stretch rate for each specimens were maintained at 0.5/s, which is in the neighborhood of instantaneous states for all the materials (Section 4.1.2). In this situation, all the tests presented in Section 2.6 illustrate the fundamental stress relaxation phenomena of the materials from the instantaneous to the equilibrium state and thus include the entire viscosity

domain. To find an adequate value of η , numerical trials of the rate-dependent hyperelastic model (Section 3.2) were carried out and experimental data were compared with those of numerical results. For NR-I and NR-II, $\eta = 4.20$ and 3.50 MPa s were found to represent the relaxation feature adequately (Fig. 14(a) and (b)). In HDR, the corresponding value was 3.00 MPa s (Fig. 14(c)).

5. Performance evaluation and discussion

An improved hyperelastic relation has been presented in Section 3.1 and the new relation has been incorporated in a rate-dependent model structure in Section 3.2. On the basis of the experimental observation presented in Section 2, a physically meaningful parameter identification scheme has been presented in Section 4. In this section, the proposed hyperelastic model is compared with conventional ones in representing

equilibrium and instantaneous responses of NR and HDR under compression. Finally, the parameters determined in Section 4 were used in the rate-dependent constitutive model to verify the adequacy of the proposed parameter identification scheme.

5.1. Conventional hyperelastic relations and comparative performances

Among W functions based on the statistical molecular theory, Arruda and Boyce (1993) function is the most successful one. The strain energy function is expressed in terms of I_1 and needs only two parameters, namely μ and λ_m

$$W(I_1) = \mu \left\{ \frac{1}{2}(I_1 - 3) + \frac{1}{20\lambda_m^2}(I_1^2 - 9) + \frac{11}{1050\lambda_m^4}(I_1 - 27)^3 + \dots \right\}. \quad (16)$$

Among the strain-invariant based models, a polynomial form of energy density relation proposed by Rivlin (1948) is the first and the commonest one. Eq. (17) depicts the general polynomial form with C_{ij} as material parameter

$$W(I_1, I_2) = \sum_{i,j} C_{ij}(I_1 - 3)(I_2 - 3). \quad (17)$$

The most commonly referred Mooney–Rivlin function (Mooney, 1940; Rivlin, 1948) is derived as the first order polynomial expansion of Eq. (17)

$$W(I_1, I_2) = C_{10}(I_1 - 3) + C_{01}(I_2 - 3). \quad (18)$$

However, the large strain-hardening feature of rubbers cannot be modeled with this expression and prompted other contemporary researchers to include different forms of I_2 . In this course, after following the proposal of Rivlin and Saunders (1951), Hart-Smith and Crisp (1967) proposed a modified form of expression with C_1 , C_2 , and C_3 as material parameters:

$$W(I_1, I_2) = C_1 \int \exp\{C_3(I_1 - 3)^2\} dI_1 + C_2 \ln \left(\frac{I_2}{3} \right). \quad (19)$$

Subsequently, Alexander (1968) improved the Hart-Smith function and included a more complicated form of expression of I_2 with C_1 , C_2 , and C_3 as material parameters

$$W(I_1, I_2) = C_1 \int \exp\{C_3(I_1 - 3)^2\} dI_1 + C_2 \ln \left(\frac{(I_2 - 3) + \gamma}{\gamma} \right) + C_3(I_2 - 3). \quad (20)$$

In this course, Tschoegl (1972) suggested to take some higher order terms of original Rivlin expression (Eq. (17)) for further correction of Mooney–Rivlin function. Yeoh (1990) adopted this idea and finally came out with a cubic function of I_1

$$W(I_1) = C_{10}(I_1 - 3) + C_{20}(I_1 - 3)^2 + C_{30}(I_1 - 3)^3, \quad (21)$$

where C_{10} , C_{20} , and C_{30} are material parameters.

Apart from all these approaches, Yamashita and Kawabata (1992) considered strip-biaxial and bi-axial test results and proposed another representation of W with C_5 , C_2 , C_3 , and N as material parameters

$$W(I_1, I_2) = C_5(I_1 - 3) + C_2(I_2 - 3) + \frac{C_3}{N+1}(I_1 - 3)^N. \quad (22)$$

The performance of the proposed W relation in comparison with the conventional hyperelastic models in representing equilibrium and instantaneous responses is presented in Figs. 15 and 16, respectively. All material parameters in hyperelastic models are determined from experimental data with a least-squares method. In this figure, Error (%) in stress is defined by

$$\% \text{Error} = \frac{\sigma_{\text{Expt}} - \sigma_{\text{Predicted}}}{\sigma_{\text{Expt}}} \times 100, \quad (23)$$

where the Cauchy stresses obtained from experiments and theoretical prediction are expressed by σ_{Expt} and $\sigma_{\text{Prediction}}$, respectively. The comparison clearly indicates the inadequacy of the conventional models in representing the stress–stretch response at low stretch level (up to 0.85) and displays the improvement achievable with the pro-

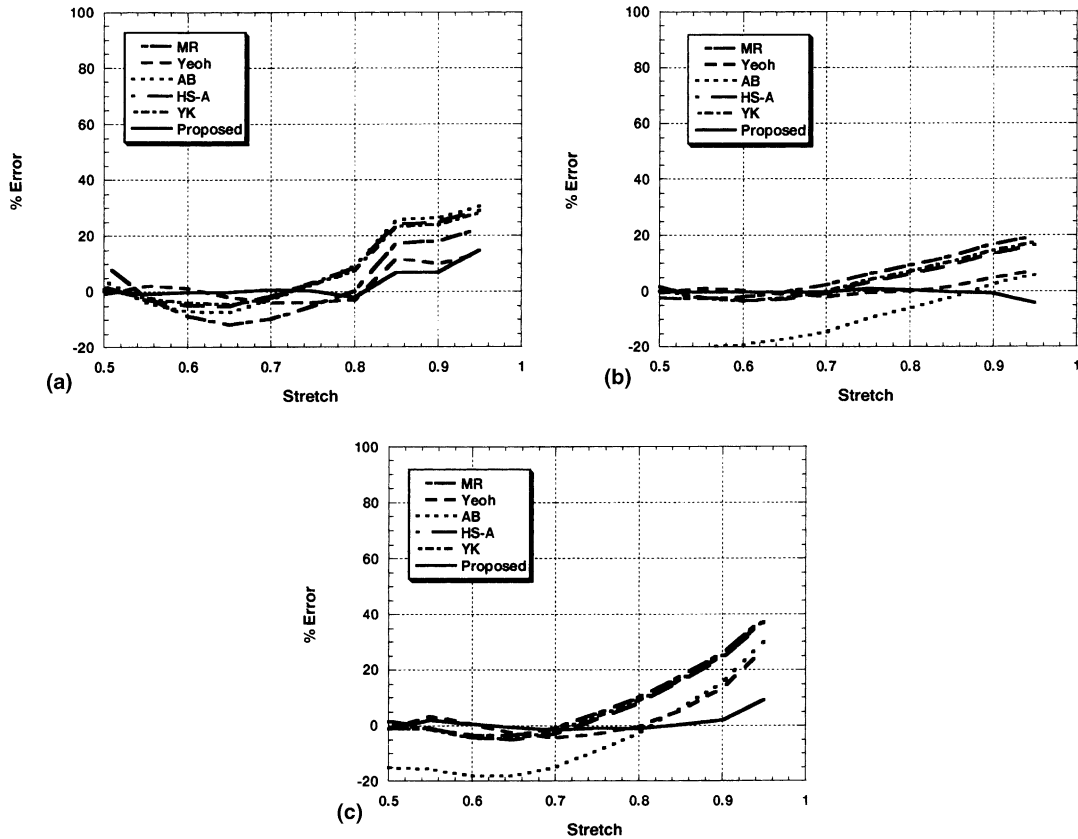


Fig. 15. Comparative performance of the proposed and the conventional hyperelasticity models in representing equilibrium response of: (a) NR-I, (b) NR-II, (c) HDR under compression. MR: Mooney–Rivlin model, Yeoh: Yeoh model, AB: Arruda–Boyce model, HS–A: Hart–Smith–Alexander model, YK: Yamashita–Kawabata model, proposed: proposed model.

posed model. The improvement is more remarkable in the instantaneous response representation where the high initial stiffness feature is the most prominent. However, above 0.80 stretch levels, all the models show good performance. In general, the model performed better in NR than HDR.

5.2. Numerical simulation of monotonic compression tests

The elastic and viscous parameters determined in Section 4 were used in the constitutive model presented in Section 3 to simulate the monotonic compression test at different stretch rates. Figs. 17–19 show the simulation results in comparison with experimental data for NR-I, NR-II, and HDR specimens, where a good conformity can be

observed in all the cases. The capability of the model in simulating the high initial stiffness feature at different stretch rates is well portrayed in Figs. 17 and 19. In contrast, the performance of the model in predicting the response of NR-II containing no initial stiffness feature is also noticeable in Fig. 18. Furthermore, the model also was found to show its capability in reproducing the intermediate large compression and large strain-hardening feature of all the specimens at slower and faster stretch rates. The yielding of such ability is due to the inclusion of the newly proposed hyperelastic relation in the finite deformation rate-dependent model and the adequacy of the proposed parameter identification procedure.

However, in all the specimens, the simulation result at 0.001/s stretch rate is slightly poorer than

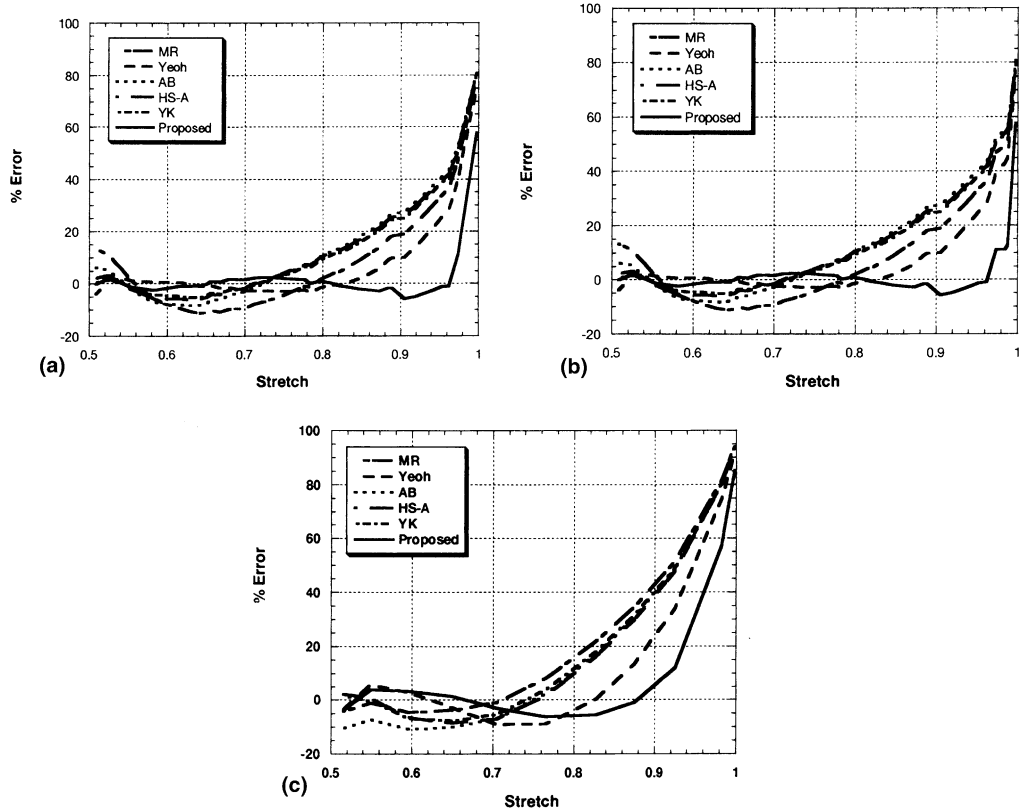


Fig. 16. Comparative performance of the proposed and the conventional hyperelasticity models in representing instantaneous response of: (a) NR-I, (b) NR-II, (c) HDR under compression. MR: Mooney–Rivlin model, Yeoh: Yeoh model, AB: Arruda–Boyce model, HS-A: Hart–Smith–Alexander model, YK: Yamashita–Kawabata model, proposed: proposed model.

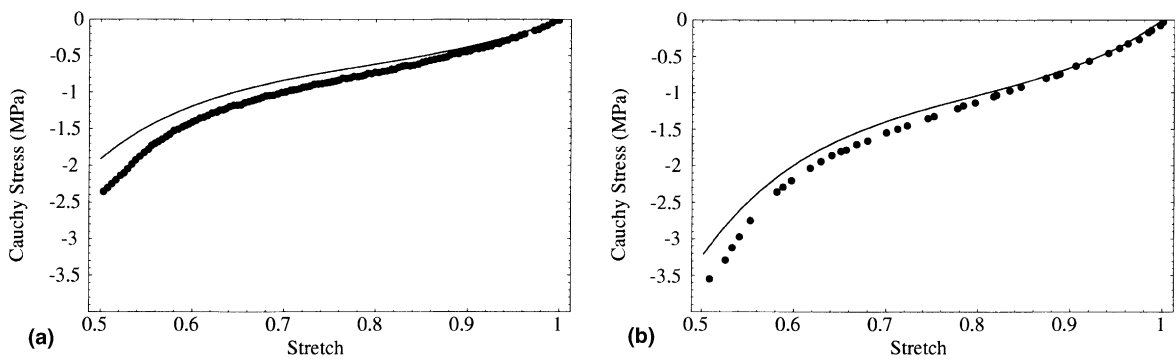


Fig. 17. Numerical simulation of monotonic compression test at different stretch rates for NR-I: (–) Numerical simulation, (•) experiment. (a) 0.001, (b) 0.47 s⁻¹ stretch rates.

those of other faster stretch rate cases (Figs. 17–19). This tendency might be related to the limitation of present viscosity modeling, where only one

linear viscosity parameter is employed to model the rate-dependent behavior. From the comparison of relaxation curves shown in Fig. 14, the test

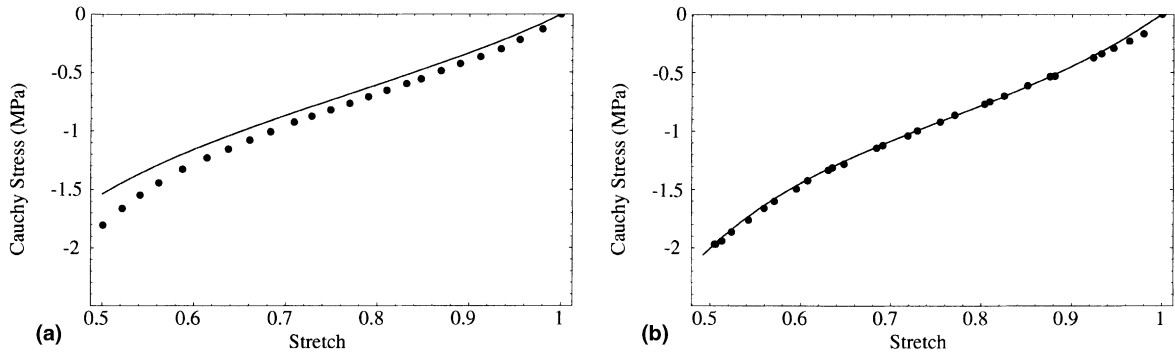


Fig. 18. Numerical simulation of monotonic compression test at different stretch rates for NR-II: (–) numerical simulation, (●) experiment. (a) 0.001, (b) 0.65 s^{-1} stretch rates.

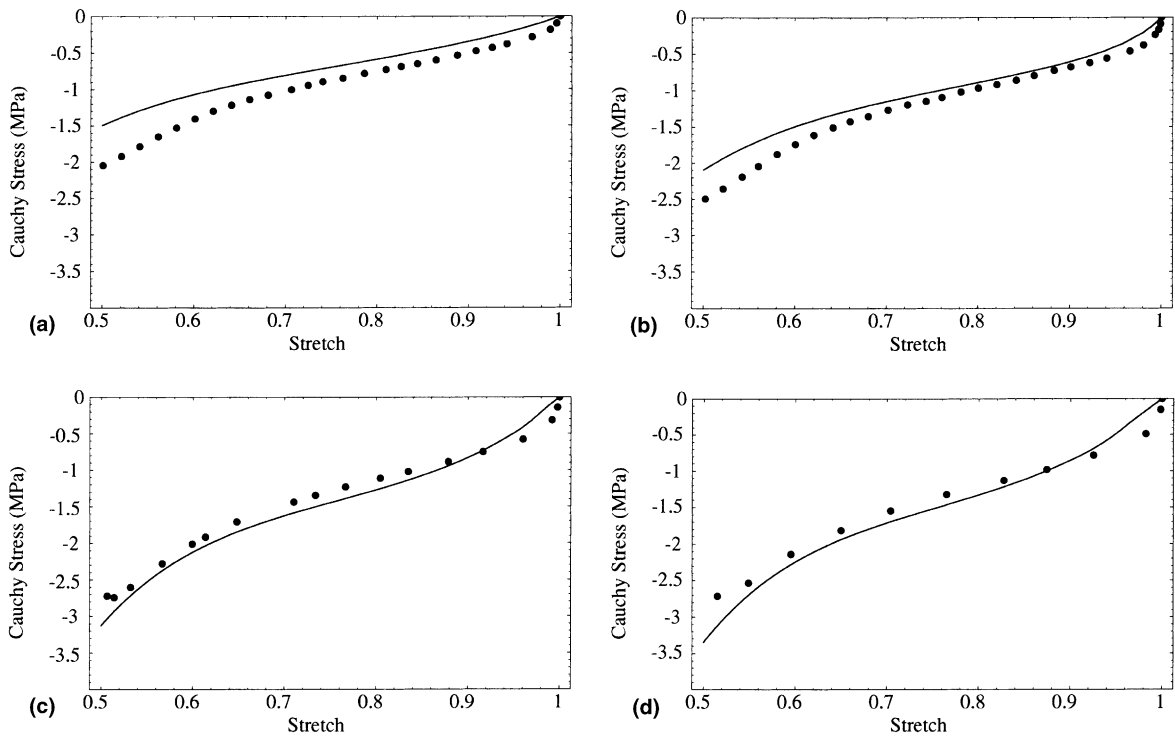


Fig. 19. Numerical simulation of monotonic compression test at different stretch rates for HDR: (–) numerical simulation, (●) experiment. (a) 0.001, (b) 0.073, (c) 0.47, (d) 0.88 s^{-1} stretch rates.

results for NR-I and HDR exhibit relatively fast rate of stress relaxation within the first 2 sec. followed by slow relaxation rate. This suggests non-linear dependence of the viscosity parameter or necessity of employing more than one linear viscosity parameters in the overstress branch of the

viscoelastic model. Furthermore, in the present study, the viscosity parameter for the model was determined based on the first 10–15 s. of the relaxation test history. In contrast to this, the duration of a monotonic compression test at a slow stretch rate up to 0.5 stretch level can last even for

500 s. This duration lies much beyond the range of considered length of relaxation test history.

6. Conclusion and further remarks

1. The equilibrium response of rubbers can be approximated from a multi-step relaxation test. Conducting a series of constant-rate monotonic compression tests at different stretch rates can approximate the approach of instantaneous state.
2. The proposed hyperelastic model can adequately represent the equilibrium and instantaneous states. When the elastic parameters of the material are known, the viscosity parameter can be estimated by comparing the simple relaxation test data with numerical results obtained from the finite deformation viscoelastic model.
3. A comparative performance evaluation has illustrated the better performance of the proposed hyperelastic model than the conventional ones in predicting the high initial stiffness present in the response of NR and HDR under compression.
4. The comparison of numerical results with those of monotonic compression test results for different stretch rate cases indicates the adequacy of the proposed model and parameter identification procedure. However, the present work has suggested for considering nonlinear dependence of viscosity in NR and HDR to improve the prediction capability. It is the present interest of the authors to address this aspect.

Acknowledgements

The authors are indeed grateful to Professor H. Horii, Department of Civil Engineering, University of Tokyo, Japan, for his valuable comments and suggestions and particularly for extending the experimental facilities of his laboratory to carry out the mechanical tests of the investigation. The authors gratefully acknowledge the kind cooperation extended by the Yokohama Rubber Co. by providing test specimens. The authors also sincerely recall the funding provided by the Japanese

Ministry of Education, Science, Sports and Culture as Grant-in-Aid for Scientific Research (C) (No. 12650457) to carry out this research.

References

- Aklonis, J.J., Macnight, W.J., Shen, M., 1972. *Introduction to Polymer Viscoelasticity*. John Wiley & Sons, Canada.
- Alexander, H., 1968. A constitutive relation for rubber-like materials. *Int. J. Eng. Sci.* 6, 549–563.
- Arruda, E.M., Boyce, M.C., 1993. A three-dimensional constitutive model for the large stretch behavior of rubber elastic materials. *J. Mech. Phys. Solids* 41 (2), 389–412.
- Bergstrom, J.S., Boyce, M.C., 1998. Constitutive modeling of the large strain time-dependent behavior of elastomers. *J. Mech. Phys. Solids* 46 (5), 931–954.
- Bonet, J., Wood, R.D., 1997. *Nonlinear Continuum Mechanics for Finite Element Analysis*. Cambridge University Press, Cambridge.
- Bueche, F., 1961. Mullins effect and rubber-filler interaction. *J. Appl. Polym. Sci.* 5 (15), 271–281.
- Castellani, A., Kajon, G., Panjeri, P., Pezzoli, P., 1998. Elastomeric materials used for vibration isolation of railway lines. *J. Eng. Mech.* 124, 614–621.
- Charlton, D.J., Yang, J., Teh, K.K., 1993. A review of methods to characterize rubber elastic behavior for use in finite element analysis. *Rubber Chem. Technol.* 67, 481–503.
- Dorfmann, A., Burtcher, S.L., 2000. Aspects of cavitation damage in seismic bearings. *J. Struct. Eng., ASCE* 126, 573–579.
- Gent, A.N., 1962. Relaxation processes in vulcanized rubber. I. relation among stress relaxation, creep, recovery, and hysteresis. *J. Appl. Polym. Sci.* 6 (22), 433–441.
- Hart-Smith, L.J., 1966. Elasticity parameters for finite deformations of rubber-like materials. *Z. Angew. Math. Phys.* 17, 608–626.
- Hart-Smith, L.J., Crisp, J.D.C., 1967. Large elastic deformations of thin rubber membranes. *Int. J. Engrg. Sci.* 5, 1–24.
- Hernandez Jr., J.Y., 1998. Modeling of highly-deformable polymeric damping materials for use in seismic protective devices. Master of Science Thesis, Department of Civil and Environmental Engineering, Saitama University, Japan.
- Huber, N., Tsakmakis, C., 2000. Finite deformation viscoelasticity laws. *Mech. Mater.* 32, 1–18.
- Kawabata, S., Kawai, H., 1977. Strain energy density functions of rubber vulcanizates from biaxial extension. *Adv. Polym. Sci.* 24, 90–124.
- Kawabata, S., Matsuda, M., Tei, K., Kawai, H., 1981. Experimental survey of the strain energy density function of isoprene rubber vulcanizate. *Macromolecules* 14, 154–162.
- Kelly, J.M., 1997. *Earthquake Resistant Design with Rubber*. Springer-Verlag, London.

- Lambert-Diani, J., Rey, C., 1999. New phenomenological behavior laws for rubbers and thermo plastic elastomers. *Eur. J. Mech./Solids* 18, 1027–1043.
- Le Tallac, P., Rahier, C., Kaiss, A., 1993. Three dimensional incompressible viscoelasticity in large strain formulation and numerical approximation. *Comput. Meth. Appl. Mech. Engrg.* 109, 233–258.
- Lion, A., 1996. A constitutive model for carbon black filled rubber: experimental investigations and mathematical representation. *Continuum Mech. Thermodyn.* 8, 153–169.
- Lion, A., 1997. A physically based method to represent the thermo-mechanical behavior of elastomers. *Acta Mech.* 123, 1–25.
- Lubliner, J., 1985. A model for rubber viscoelasticity. *Mech. Res. Comm.* 12, 93–99.
- Miehe, C., Keck, J., 2000. Superimposed finite elastic-viscoelastic-plastoelastic stress response with damage in filled rubbery polymers. Experiments, modeling and algorithmic implementation. *J. Mech. Phys. Solids* 48, 323–365.
- Mooney, M., 1940. A theory of large elastic deformation. *J. Appl. Phys.* 11, 582–592.
- Mullins, L., 1969. Softening of rubber by deformations. *Rubber Chem. Technol.* 42, 339–362.
- Ogden, R.W., 1984. *Non-linear Elastic Deformations*. Ellis Horwood Ltd., Chichester.
- Peeters, F.J.H., Kussner, M., 1999. Material law selection in the finite element simulation of rubber-like materials and its practical application in the industrial design process. In: Dorfmann, A., Muhr, A. (Eds.), *Constitutive Models for Rubber*. A.A. Balkema, Rotterdam, pp. 29–36.
- Peng, T.J., Landel, R.F., 1972. *J. Appl. Phys.* 43, 3064.
- Reese, S., Govindjee, S., 1998. A theory of finite viscoelasticity and numerical aspects. *Int. J. Solids Structures* 35, 3455–3482.
- Rivlin, R.S., Saunders, D.W., 1951. Large elastic deformations of isotropic materials VII. Experiments on the deformation of rubber. *Phil. Trans. Roy. Soc.* 243, 251–288.
- Rivlin, R.S., 1948. *Philos. Trans. R. Soc. London A* 241, 379.
- Roeder, C.W., Stanton, J.F., 1983. Elastomeric bearings: state-of-the-art. *J. Struct. Eng., ASCE* 109 (12), 2853–2871.
- Truesdell, C., Noll, W., 1992. *The Non-linear Field Theories of Mechanics*, second ed. Springer-Verlag, Berlin.
- Tschoegl, N.W., 1972. Constitutive equations for elastomers. *Rubber Chem. Technol.* 45, 60–70.
- Ward, I.M., 1985. *Mechanical Properties of Solid Polymers*. John Wiley & Sons, New York.
- Yamashita, Y., Kawabata, S., 1992. Approximated form of the strain energy density function of carbon-black filled rubbers for industrial applications. *J. Soc. Rubber Ind. (Jpn)* 65 (9), 517–528 (in Japanese).
- Yeoh, O.H., 1990. Characterization of elastic properties of carbon-black filled rubber vulcanizates. *Rubber Chem. Technol.* 63, 792–805.